

## CELL BIOLOGY

# m<sup>6</sup>A mRNA modification maintains colonic epithelial cell homeostasis via NF-κB-mediated antiapoptotic pathway

Ting Zhang<sup>1,2,3†</sup>, Chenbo Ding<sup>1,2\*†</sup>, Huifang Chen<sup>1,2†</sup>, Jun Zhao<sup>4</sup>, Zhejun Chen<sup>1</sup>, Baiwen Chen<sup>1</sup>, Kaiqiong Mao<sup>1,2</sup>, Yajuan Hao<sup>1,2</sup>, Manolis Roulis<sup>5</sup>, Hao Xu<sup>5</sup>, Yuval Kluger<sup>4</sup>, Qiang Zou<sup>1</sup>, Youqiong Ye<sup>1</sup>, Meixiao Zhan<sup>6\*</sup>, Richard A. Flavell<sup>5,7\*</sup>, Hua-Bing Li<sup>1,2,5\*</sup>

Colonic mucosal barrier dysfunction is one of the major causes of inflammatory bowel disease (IBD). However, the mechanisms underlying mucosal barrier dysfunction are poorly understood. N<sup>6</sup>-methyladenosine (m<sup>6</sup>A) mRNA modification is an important modulator of epitranscriptional regulation of gene expression, participating in multiple physiological and pathological processes. However, the function of m<sup>6</sup>A modification in colonic epithelial cells and stem cells is unknown. Here, we show that m<sup>6</sup>A modification is essential for maintaining the homeostatic self-renewal in colonic stem cells. Specific deletion of the methyltransferase 14 (*Mettl14*) gene in mouse colon resulted in colonic stem cell apoptosis, causing mucosal barrier dysfunction and severe colitis. Mechanistically, we revealed that *Mettl14* restricted colonic epithelial cell death by regulating the stability of *Nfkb1a* mRNA and modulating the NF-κB pathway. Our results identified a previously unidentified role for m<sup>6</sup>A modification in colonic epithelial cells and stem cells, suggesting that m<sup>6</sup>A modification may be a potential therapeutic target for IBD.

## INTRODUCTION

The intestinal tract is the most rapidly self-renewing tissue in adult mammals. It functions both in nutrient absorption and as a barrier that protects against environmental insults. The single-layered, repetitive crypt-villus unit (1) of the intestinal epithelium consists of constantly proliferating stem cells and postmitotic cells and is critical for the maintenance of intestinal function. At the base of the crypt, continuously proliferating stem cells divide into transit-amplifying (TA) cells. TA cells, after dividing four to five times (2), differentiate into postmitotic absorptive and secretory epithelial cells. Absorptive enterocytes, also called colonocytes in the colon, characterized by a brush border, are responsible for nutrient uptake. Goblet cells, Paneth cells, enteroendocrine cells, and tuft cells belong to the secretory cell class. Goblet cells secrete mucins, which are highly glycosylated proteins that protect against mechanical stress (3). Paneth cells reside only in the base of the crypt in the small intestine and form a niche essential for the maintenance of stem cells (4), while in the colon deep crypt secretory (DCS) cells, which express regenerating family member 4 (REG4) (5), serve the same role as Paneth cells in the small intestine. Enteroendocrine cells are scattered throughout the intestinal mucosa and critically regulate metabolism and digestion (6). Tuft cells, a rare cell type (7), are involved in immune regulation.

The constant supply of all types of intestinal epithelial cells relies on a complex regulation of intestinal stem cell self-renewal and differentiation. Despite the robust regeneration of intestinal stem cells, intestinal homeostasis can be disrupted upon severe acute and chronic damage, which can lead to inflammatory bowel disease (IBD) (8), such as Crohn's disease and ulcerative colitis. The mechanism of the rapid and proper restoration of the integrity of the epithelial barrier is largely unknown.

The nuclear factor κB (NF-κB) transcription factor complex includes five members, namely, RelA (p65), RelB, c-Rel, NF-κB1 (p50), and NF-κB2 (p52). These proteins play important function in the immune response and cell survival by targeting proinflammatory genes, antiapoptotic proteins, and angiogenesis regulators. In resting cells, the p65-p50 complex (9) is inactivated by binding one of the inhibitory κB (IκB) proteins, such as IκBα (also called NFKBIA), IκBβ, or IκBε (10). When stimulated by bacterial products, such as lipopolysaccharide or host cytokines like tumor necrosis factor α (TNFα), IκBs are phosphorylated by the IκB kinase (IKK) complex and degraded by the proteasome, leading to the release of p65 and p50. Nuclear translocation of p65 and p50 then triggers NF-κB-related gene transcription (11). Depletion of NF-κB in immune cells leads to disruption of the immune response (12), while inhibition of NF-κB in intestinal epithelial cells activates cell death pathways (13). Furthermore, in intestinal epithelial cells, knockout (KO) of IKKβ failed to prevent dextran sulfate sodium (DSS)-induced inflammation and resulted in apoptosis, while in myeloid cells the loss of IKKβ decreased the expression of proinflammatory cytokines (14–16). In addition, mutation of the constitutively expressed form of IκB, also called NFKBIA, enhanced TNF-induced cell death in intestinal epithelial cells (17). Thus, in the intestine, NF-κB signaling has a dual function related to both cell survival and inflammation.

N<sup>6</sup>-methyladenosine (m<sup>6</sup>A) RNA modification is one of the most abundant and extensively distributed mRNA modifications (18). It modulates RNA metabolism, including decay, translation, localization, and splicing (19, 20). m<sup>6</sup>A modification of mRNA is performed

Copyright © 2022 The Authors, some rights reserved; exclusive licensee American Association for the Advancement of Science. No claim to original U.S. Government Works. Distributed under a Creative Commons Attribution NonCommercial License 4.0 (CC BY-NC).

<sup>1</sup>Shanghai Institute of Immunology, State Key Laboratory of Oncogenes and Related Genes, Shanghai Jiao Tong University School of Medicine, Shanghai 200025, China.

<sup>2</sup>Shanghai Jiao Tong University School of Medicine–Yale Institute for Immune Metabolism, Shanghai Jiao Tong University School of Medicine, Shanghai 200025, China. <sup>3</sup>Renji Hospital affiliated to Shanghai Jiaotong University School of Medicine, Shanghai 200127, China. <sup>4</sup>Department of Pathology, Yale University School of Medicine, New Haven, CT 06520-8055, USA. <sup>5</sup>Department of Immunobiology, Yale University School of Medicine, New Haven, CT 06520-8055, USA. <sup>6</sup>Zhuhai Interventional Medical Center, Zhuhai Precision Medical Center, Zhuhai People's Hospital, Zhuhai Hospital of Jinan University, Zhuhai, Guangdong 519000, China. <sup>7</sup>Howard Hughes Medical Institute, Yale University School of Medicine, New Haven, CT 06520-8055, USA.

\*Corresponding author. Email: chenbo.ding@sjtu.edu.cn (C.D.); zhanmeixiao1987@126.com (M.Z.); richard.flavell@yale.edu (R.A.F.); huabing.li@shsmu.edu.cn (H.-B.L.)

†These authors contributed equally to this work.

by a methyltransferase complex composed of methyltransferase-like 3 (METTL3), METTL14, and Wilms' tumor 1–associating protein (WTAP). m<sup>6</sup>A modification is erased by two demethylases, which are fat mass- and obesity-associated protein (FTO) (21) and  $\alpha$ -ketoglutarate–dependent dioxygenase AlkB homolog 5 (ALKBH5) (22). In the methyltransferase complex, METTL3 is the only catalytically active subunit, METTL14 is essential for substrate recognition, and WTAP interacts with METTL3 and METTL14 to regulate m<sup>6</sup>A deposition (23, 24). Emergent evidence has revealed that m<sup>6</sup>A modification is indispensable for the development of embryonic stem cells (25), hematopoietic stem cells (26), T cells (27, 28), and neural cells (29). Moreover, dysfunctional m<sup>6</sup>A modification is involved in the development of human acute myeloid leukemia (30) and other cancers (31). However, how m<sup>6</sup>A modification regulates the function of colonic epithelial cells is still unclear. Although previous work demonstrated that an m<sup>6</sup>A reader protein, YTH domain-containing family protein 1 (YTHDF1), drives Wnt-related intestinal regeneration and tumorigenesis; however, YTHDF1 is dispensable for normal intestinal development in mice and YTHDF1 depletion does not affect body weight and crypt-villus architecture (32). Other reports published recently showed the promotive role of METTL3 in colorectal cancer (CRC) (33, 34); however, the significance of m<sup>6</sup>A modification in colonic epithelial cells under physiological conditions remains to be determined.

Here, we report that, in the steady state, m<sup>6</sup>A modification is indispensable for the maintenance of colonic epithelial homeostasis. Mice with colon-specific KO of *Mettl14* showed disturbed integrity of the colonic epithelial barrier, resulting in severe colitis. The mRNA of *Nfkb1a*, the NF- $\kappa$ B inhibitor, is the direct target of m<sup>6</sup>A modification. Thus, depletion of m<sup>6</sup>A modification led to enhanced stability of *Nfkb1a* mRNA and accumulation of NFKB1A protein, which down-regulated the NF- $\kappa$ B–mediated antiapoptotic pathway and promoted colonic cell death.

## RESULTS

### Deletion of *Mettl14* in colonic epithelial cells leads to a wasting phenotype and spontaneous colitis

We first investigated the dynamic changes in m<sup>6</sup>A levels in colonic epithelial cells during mouse development. The global m<sup>6</sup>A level in intestinal mRNAs was lower in adult 8-week-old mice than at 2 weeks after birth (fig. S1A), implying an important function of m<sup>6</sup>A modification in the development of colonic epithelial cells. To investigate the genetic requirement for *Mettl14* in colonic epithelial cells, we conditionally deleted *Mettl14* by generating *Villin-cre*<sup>+</sup>; *Mettl14*<sup>ff</sup> (hereafter called *Mettl14* KO) mice (fig. S1B), in which the *Vil1* gene promoter–driven Cre recombinase would specifically delete the floxed *Mettl14* gene in all intestinal epithelial cells. The *Mettl14* KO efficiency was confirmed by genotyping, quantitative reverse transcription polymerase chain reaction (qRT-PCR) (fig. S1C), and immunohistochemistry (fig. S1, D and E). Consequently, the total m<sup>6</sup>A level in mRNAs in the *Mettl14* KO group was decreased in comparison with *Mettl14*<sup>ff</sup> littermates [hereafter called *Mettl14* wild type (WT)], as verified by m<sup>6</sup>A dot blot (fig. S1F).

At 2 weeks of age, *Mettl14* KO mice were distinguishable from *Mettl14* WT due to their notable growth retardation (Fig. 1A). From 2 to 8 weeks, *Mettl14* KO mice demonstrated lower weight gains (Fig. 1B) than *Mettl14* WT mice. This difference was associated with a shorter colon in the *Mettl14* KO mice (Fig. 1C). Furthermore,

*Mettl14* KO mice developed diarrhea as early as at 2 weeks of age (Fig. 1D). The decrease in the global level of m<sup>6</sup>A mRNA modification in colonic epithelial cells from infancy to adulthood suggests that m<sup>6</sup>A modification deficiency has a significant impact on the developing colon. Furthermore, mouse survival was monitored. We observed a significantly lower survival in *Mettl14* KO mice, and the mortality reached its peak in mice around 3 or 4 weeks old, ranging from 42.86 to 64.29% (Fig. 1E). However, no mice died after the age of 4 weeks, consistent with the data showing that *Mettl14* KO mice have the greatest suppression of weight gain at around 3 or 4 weeks of age. Detailed autopsy of the *Mettl14* KO mice revealed a shorter colon that was filled with bloody feces (Fig. 1F). To further explore the impact of *Mettl14* depletion on the changes in the morphology of intestinal epithelial cells, hematoxylin and eosin (H&E) and Muc2 staining was performed in mice of different ages. Aggravated deterioration of the colon was detected from 2 to 8 weeks of age, which was characterized by the loss of goblet cells, crypt architectural distortion, inflammatory cell infiltration, and epithelial ulceration (Fig. 1, G to J). However, we found no significant changes in the length of small intestine, the length of villus, and the integrity of crypts, nor with the relative expression of specific markers of different cell subsets between the two groups (fig. S2, A to E). These results reveal that METTL14-mediated m<sup>6</sup>A modification plays an important role in the development of colonic epithelial cells, and depletion of *Mettl14* triggers a wasting phenotype in the infant stage followed by spontaneous colitis.

### *Mettl14* depletion leads to colonic epithelial cell death

To address how *Mettl14* deficiency affects the function of different types of colonic epithelial cells, we first examined the expression of genes encoding specific markers of total colonic epithelial cells, stem cells, goblet cells, and colonocytes (Fig. 2A). All these marker genes were down-regulated in *Mettl14* KO mice compared to their WT littermates, suggesting that the KO of *Mettl14* affects all types of colonic epithelial cells in the 2-week-old mice. Mucus production by goblet cells serves as an indispensable barrier controlling the microbiome in the colon (3), which could be specifically stained by Alcian blue–periodic acid–Schiff (AB-PAS) and Muc2. AB-PAS and Muc2 staining also showed that *Mettl14* KO mice exhibited a smaller number of goblet cells than the WT controls (Fig. 2, B and C). To determine whether the loss of colonic epithelial cells was due to decreased cell survival, we performed the terminal deoxynucleotidyl transferase–mediated deoxyuridine triphosphate nick end labeling (TUNEL) cell death assay on colon sections and found higher numbers of TUNEL-positive cells in the *Mettl14* KO group than in the *Mettl14* WT group (Fig. 2, D and E). Furthermore, the proportion of cleaved caspase-3–positive cells in the colon was higher in the *Mettl14* KO group than in the *Mettl14* WT group (Fig. 2, F and G). Subsequently, we performed Ki67 staining to further evaluate whether *Mettl14* deficiency could also affect cell proliferation. Although no significant difference was found in cell proliferation between the WT and KO groups (Fig. 2, H and I), the cell apoptosis versus proliferation ratio was much higher in *Mettl14* KO mice compared to the WT controls (Fig. 2J). The expression of both CD3 and CD11B in the *Mettl14* KO group was comparable to that in the *Mettl14* WT group, excluding the presence of ongoing inflammation in the 2-week-old mice (fig. S3, A to D). Together, these data document that m<sup>6</sup>A modification and *Mettl14* are critical for the maintenance of colonic epithelial cell homeostasis by restricting cell death.

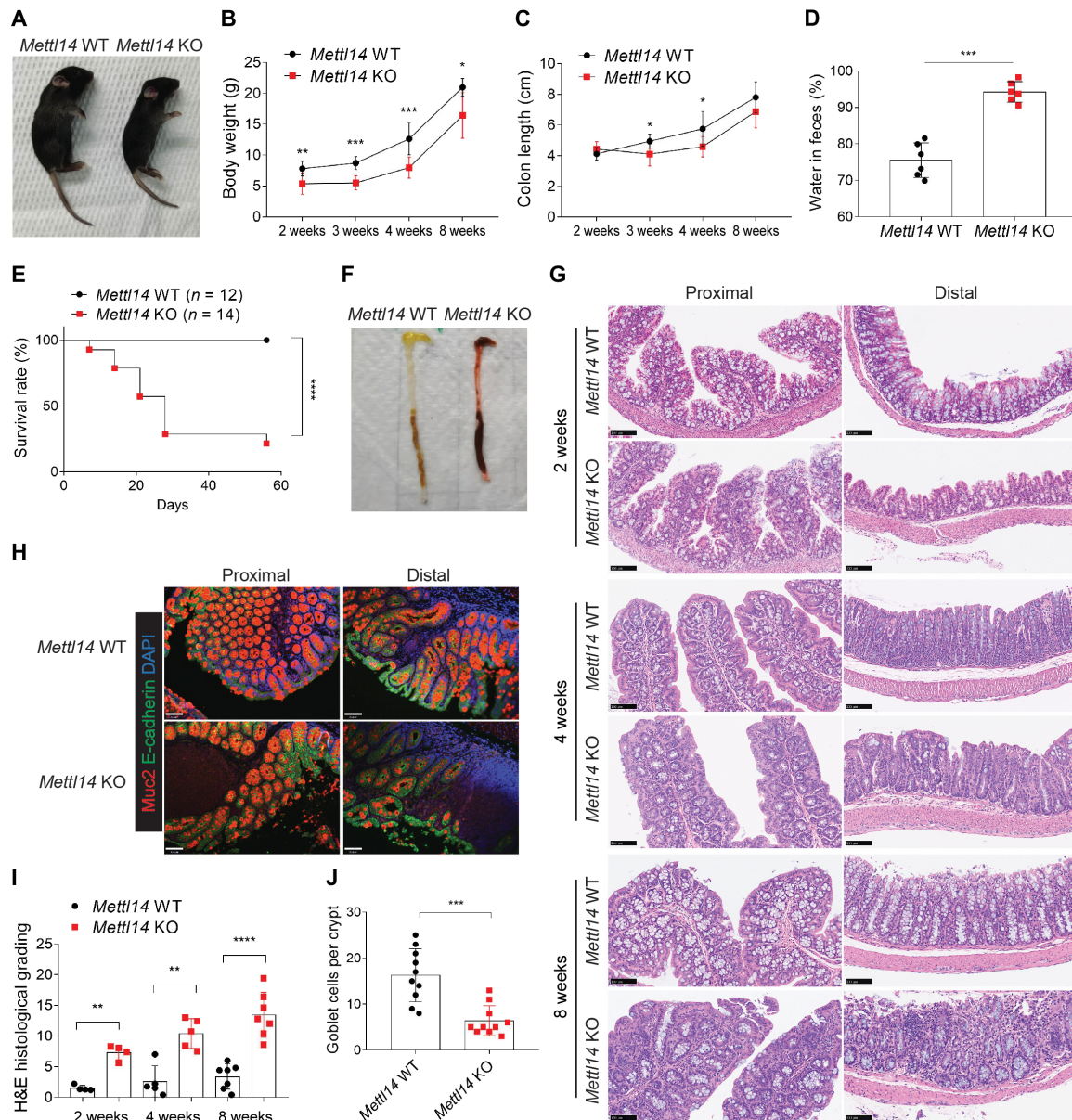


**Fig. 1. *Mettl14* depletion in intestinal epithelial cells triggers a wasting phenotype and spontaneous colitis.** (A) Representative image of *Mettl14* WT and *Mettl14* KO mice at 2 weeks of age. (B and C) Body weight [(B),  $n = 5$  to 8 per group] and colon length [(C),  $n = 6$  to 10 per group] of *Mettl14* WT and *Mettl14* KO mice from 2 to 8 weeks. (D) Fecal water content of *Mettl14* WT and *Mettl14* KO mice at 2 weeks of age ( $n = 6$  per group). (E) Survival rate of *Mettl14* WT ( $n = 12$ ) and *Mettl14* KO ( $n = 14$ ) mice was observed from 2 to 8 weeks, and the corresponding survival curves were plotted. (F) Representative image of autopsies from *Mettl14* WT and *Mettl14* KO colon. (G) Representative H&E staining of proximal and distal colon sections from *Mettl14* WT and *Mettl14* KO mice at 2, 4, and 8 weeks of age (scale bars, 100  $\mu\text{m}$ ). (H) Representative Muc2 staining of proximal and distal colon sections from *Mettl14* WT and *Mettl14* KO mice at 8 weeks of age (scale bars, 70  $\mu\text{m}$ ). (I and J) Quantitative analysis of H&E score [(I),  $n = 4$  to 7 per group] and the number of goblet cells [(J),  $n = 10$  per group]. Data are presented as means  $\pm$  SD. Two-sided Student's *t* test (B to D, I, and J) and log-rank (Mantel-Cox) test (E) were performed (\* $P < 0.05$ ; \*\* $P < 0.01$ ; \*\*\* $P < 0.001$ ; \*\*\*\* $P < 0.0001$ ).

### Single-cell RNA sequencing reveals colonic stem cell dysfunction in *Mettl14* KO mice

To investigate the heterogeneity of colonic epithelial cells and identify the impact of  $m^6\text{A}$  deficiency on distinct types of epithelial cells, we performed single-cell RNA sequencing (scRNA-seq) analysis. Through sequencing 7863 epithelial cells, we identified a total of seven clusters of colonic epithelial cell types using *t*-distributed stochastic neighborhood embedding (*t*-SNE) (Fig. 3A) and labeled

each cluster by the expression of known marker genes (fig. S4, A to H), including stem cells, TA cells, DCS cells, tuft cells, colonocytes, enteroendocrine cells, and goblet cells. Subsequently, we defined a gene expression signature for each cell type using our scRNA-seq data, highlighting known markers (Fig. 3B). By splitting these cells into *Mettl14* WT and *Mettl14* KO groups (fig. S5, A and B), we observed a difference in cellular composition between the two groups (Fig. 3C). In the *Mettl14* KO group, the proportion of stem cells,

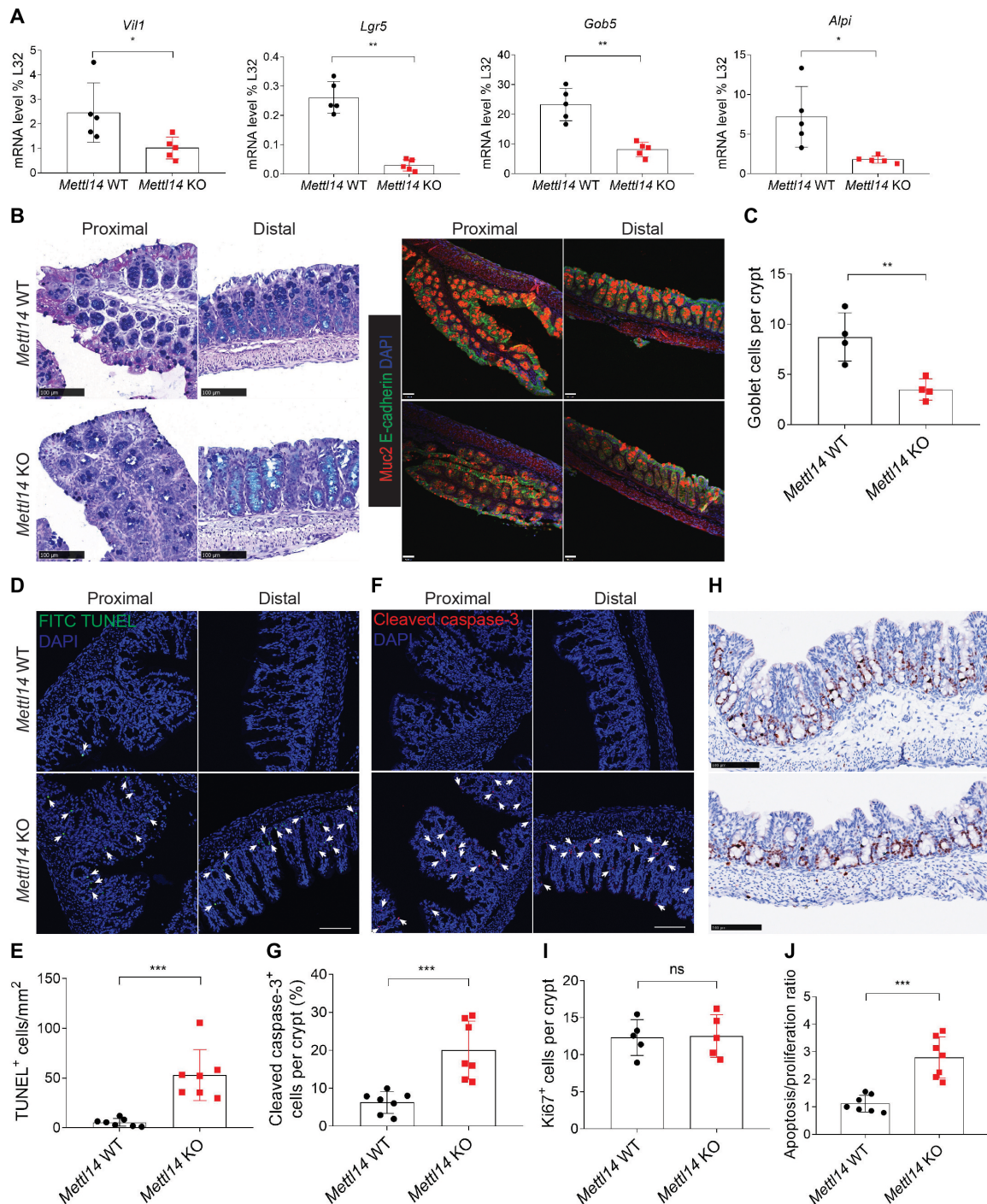


**Fig. 2. *Mettl14* depletion leads to colonic epithelial cell death.** (A) qRT-PCR analysis of gene expression in *Mettl14* WT and *Mettl14* KO mice at 2 weeks of age. *Vil1*, intestinal epithelial cell marker; *Lgr5*, intestinal stem cell marker; *Gob5*, goblet cell marker; *Alpi*, colonocyte marker ( $n = 4$  to 5 per group). (B) Left: Representative AB-PAS-stained proximal and distal colon sections of *Mettl14* WT and *Mettl14* KO mice at 2 weeks of age (scale bars, 100  $\mu$ m). Right: Representative Muc2 staining of proximal and distal colon sections from *Mettl14* WT and *Mettl14* KO mice at 2 weeks of age (scale bars, 70  $\mu$ m). (C) Quantitative analysis of AB-PAS and Muc2 staining ( $n = 4$  per group). (D and E) Representative TUNEL staining of proximal and distal colon sections from *Mettl14* WT and *Mettl14* KO mice at 2 weeks of age [(D), scale bar, 100  $\mu$ m] and quantitative analysis [(E),  $n = 7$  per group]. TUNEL-positive cell (arrows). (F and G) Representative cleaved caspase-3-stained proximal and distal colon sections of *Mettl14* WT and *Mettl14* KO mice at 2 weeks of age [(F), scale bar, 100  $\mu$ m] and quantitative analysis [(G),  $n = 7$  per group]. Cleaved caspase-3-positive cell (arrows). (H and I) Representative staining of distal colon sections from *Mettl14* WT and *Mettl14* KO mice at 2 weeks of age [(H), scale bars, 100  $\mu$ m] and quantitative analysis [(I),  $n = 5$  per group]. (J) Quantitative analysis of cell apoptosis versus cell proliferation ratio ( $n = 7$  per group). Data are presented as means  $\pm$  SD. Two-sided Student's *t* test (A, C, E, G, I, and J) was performed (ns, no significance; \* $P < 0.05$ ; \*\* $P < 0.01$ ; \*\*\* $P < 0.001$ ).

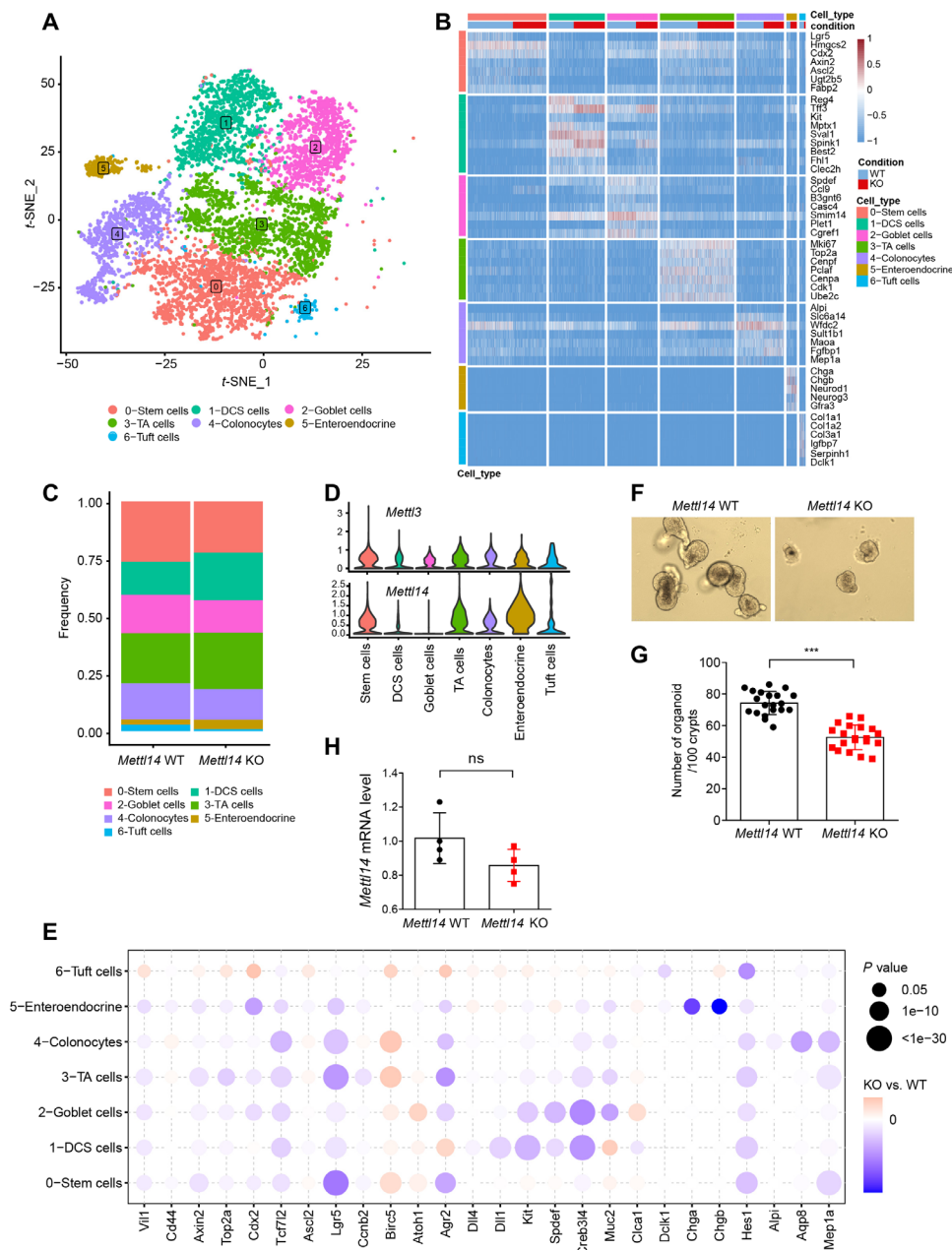


**Fig. 3. scRNA-seq reveals dysfunction of colonic epithelial cells in *Mettl14* KO mice.** (A) *t*-SNE plot of 7863 epithelial cells from *Mettl14* WT and *Mettl14* KO mouse colons of 2 weeks of age showing seven major clusters. (B) Gene expression heatmap of seven clusters. Rows represent signature genes, and columns represent different clusters. (C) Proportion of each epithelial cell cluster among the total epithelial cells. (D) Violin plots showing the entire range of *Mettl3* and *Mettl14* gene expression levels per single cell in each cluster after imputation. (E) Bubble heatmap showing expression of selected marker genes for each cluster. (F) Representative bright-field images of colonic organoids grown from *Mettl14* WT and *Mettl14* KO mice. (G) Organoid number per 100 crypts per well in 3D culture medium ( $n = 20$  for each group). (H) Statistical analysis of relative levels of *Mettl14* in surviving organoids from *Mettl14* WT and *Mettl14* KO mice ( $n = 4$  per group). Data are presented as means  $\pm$  SD. Two-sided Student's *t* test (G and H) was performed ( $***P < 0.001$ ).

goblet cells, and colonocytes was much decreased, while the population of TA cells was expanded.

In the colon, *Reg4*<sup>+</sup> DCS cells, instead of Paneth cells, are intermingled with *Lgr5*<sup>+</sup> stem cells at the crypt base and act as a stem cell niche in colonic crypts (5). It has been reported that after treatment with DSS, cells expressing high levels of *Kit* (35) and *Reg4* convert to stem-like cells in the colon (36). These findings imply that *Reg4*<sup>+</sup> DCS cells can assume the properties of stem cells after stem cell loss.

Consistently, the DCS cell population, marked by *Kit* and *Reg4* (fig. S4, C and D), was also increased in the *Mettl14* KO group (Fig. 3C). In addition, we checked the expression levels of *Mettl14* and *Mettl3* in all the clusters and found relatively higher expression of both *Mettl14* and *Mettl3* in stem cells and TA cells (Fig. 3D), implying that m<sup>6</sup>A modification mainly affects the function of stem cells and progenitor cells. Furthermore, bubble heatmap analysis demonstrated a difference in the expression of marker genes between the

*Mettl14* WT and *Mettl14* KO groups (Fig. 3E): The mRNA levels of stem cell marker (*Lgr5*), goblet cell transcription factor (*Spdef*), enteroendocrine cell marker (*Chga*), and colonocyte marker (*Alpi*) were all decreased after *Mettl14* depletion, which was consistent with the qPCR data (Fig. 2A).

As all the mature epithelial cells are derived from stem cells, we postulated that m<sup>6</sup>A modification depletion mainly disrupts the function of the epithelial stem cells and, as a result, affects the development of all the matured epithelial cells. Therefore, to directly dissect the impact of *Mettl14* depletion on the stem cell function, we isolated colonic crypts from both *Mettl14* WT and *Mettl14* KO mice and cultured them in a three-dimensional (3D) organoid growth medium. We observed that the organoid-forming efficiency of the crypts from the *Mettl14* KO group was lower than from the *Mettl14* WT group (Fig. 3, F and G), consistent with the scRNA-seq data presented above. Then, we further examined the expression level of *Mettl14* in organoids and found that *Mettl14* was not completely depleted in the surviving organoids in the KO groups (Fig. 3H), suggesting that *Mettl14*-deficient stem cells were unable to survive in organoid culture. Together, these data suggest that *Mettl14* deficiency leads to the loss of colonic stem cells, inhibiting the formation and function of the mature colonic epithelial cells.

### *Mettl14* deficiency in *Lgr5*<sup>+</sup> stem cells promotes cell apoptosis and DSS-induced colitis

Because *Lgr5* is a marker of intestinal epithelial stem cells and *Lgr5* mRNA was down-regulated, we investigated whether the m<sup>6</sup>A machinery

regulates colonic epithelial cell function by directly targeting *Lgr5* mRNA for m<sup>6</sup>A-mediated degradation. However, we did not find *Lgr5* mRNA in multiple MeRIP-seq (m<sup>6</sup>A methylated RNA immunoprecipitation sequencing) databases as 3' untranslated region (UTR) of *Lgr5* mRNA does not have the typical m<sup>6</sup>A modification consensus motifs (37).

To investigate the role of METTL14 in *Lgr5*<sup>+</sup> stem cells in vivo, we generated a mouse model with a conditional *Mettl14* KO in *Lgr5*<sup>+</sup> stem cells by crossing *Lgr5-EGFP-IRES-creERT2* (*Lgr5-creERT*) mice with floxed alleles of *Mettl14* (hereafter called *Mettl14*<sup>fl/fl</sup> *Lgr5*<sup>creERT</sup> mice). When these engineered mice were treated with tamoxifen, the *Lgr5* promoter-driven Cre recombinase specifically deleted the floxed *Mettl14* gene in *Lgr5*-expressing intestinal stem cells and their derived epithelial cell progeny. We first determined whether *Mettl14* deficiency in stem cells affected the survival of intestinal stem cells. After 7 days of tamoxifen administration, more cleaved caspase-3-positive cells were detected in *Mettl14*<sup>fl/fl</sup> *Lgr5*<sup>creERT</sup> mice than in *Mettl14*<sup>fl/fl</sup> mice (Fig. 4, A and B). It is well documented that rapidly proliferating and regenerating intestinal stem cells ensure intestinal epithelial homeostasis during injury repair. To gain a better functional insight into the effect of *Mettl14* depletion on *Lgr5*<sup>+</sup> stem cells, we treated the mice with DSS to accelerate the deterioration of intestinal epithelial cells. The *Mettl14*<sup>fl/fl</sup> *Lgr5*<sup>creERT</sup> mice developed more severe colitis than their littermates, as judged by weight loss (Fig. 4C), colon length (Fig. 4, D and E), and colitis severity score defined by endoscopy (Fig. 4F). These results demonstrate that

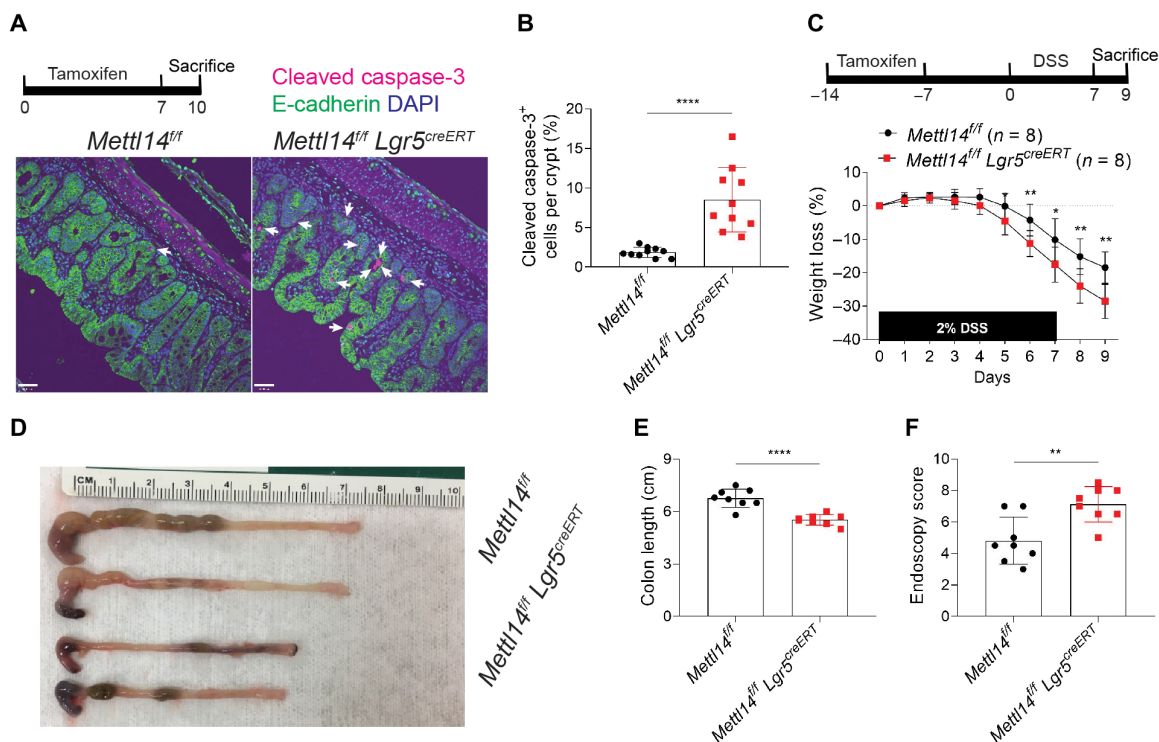


**Fig. 4. *Mettl14* deficiency in *Lgr5*<sup>+</sup> stem cells promotes cell apoptosis and DSS-induced colitis.** (A and B) *Mettl14*<sup>fl/fl</sup> *Lgr5*<sup>creERT</sup> and *Mettl14*<sup>fl/fl</sup> littermates were treated with tamoxifen daily for 7 days and then sacrificed at day 10 for cleaved caspase-3 staining. Representative cleaved caspase-3 staining of distal colon sections from *Mettl14*<sup>fl/fl</sup> *Lgr5*<sup>creERT</sup> and *Mettl14*<sup>fl/fl</sup> mice [(A); scale bars, 70 μm] and quantitative analysis [(B), *n* = 10 per group]. (C to F) To induce colitis, after treatment with tamoxifen daily for 7 days and resting for 7 days, mice were treated with 2% DSS water for a further 7 days. Weight loss of *Mettl14*<sup>fl/fl</sup> *Lgr5*<sup>creERT</sup> and *Mettl14*<sup>fl/fl</sup> mice [(C), *n* = 8 per group]. Representative photo of colon (D) and colon length measurements from *Mettl14*<sup>fl/fl</sup> *Lgr5*<sup>creERT</sup> and *Mettl14*<sup>fl/fl</sup> mice on day 9 [(E), *n* = 8 per group]. Colonoscopy severity score analysis on day 9 [(F), *n* = 8 per group]. Data are presented as means ± SD. Two-sided Student's *t* test (B) and two-tailed Mann-Whitney *U* test (C, E, and F) were performed (\**P* < 0.05; \*\**P* < 0.01; \*\*\*\**P* < 0.0001).

*Mettl14* depletion in *Lgr5*<sup>+</sup> stem cells results in increased stem cell apoptosis and increased severity of DSS-induced colitis.

### ***Mettl14* regulates colonic epithelial cell homeostasis by restricting TNF-induced cell death**

To comprehensively understand the molecular pathways by which *Mettl14*-mediated m<sup>6</sup>A modification regulates the homeostasis of colonic epithelial cells, we conducted a bulk RNA-seq analysis and compared the gene expression of the colonic epithelial cells purified from *Mettl14* KO mice and their WT littermates. The loss of *Mettl14* in epithelial cells resulted in an up-regulation of 1014 genes and down-regulation of 502 genes (Fig. 5, A and B). Kyoto Encyclopedia of Genes and Genomes (KEGG) pathway enrichment analysis showed that the differentially expressed genes were significantly enriched for pathways involved in TNF signaling and apoptosis (Fig. 5C). To reveal the major signaling pathway affected in *Mettl14* KO mice in an unbiased way, the bulk RNA-seq data were subjected to gene set enrichment analysis (GSEA). We found that the *Mettl14* KO group was enriched in signaling pathways related to TNF-induced cell death via NF-κB inhibition (Fig. 5D). It has been mentioned above that inhibition of NF-κB restricts proinflammatory signaling in myeloid cells, while the inhibition of NF-κB favors TNF-induced cell death in intestinal epithelial cells (12, 13, 38). Next, we determined the expression levels of key genes involved in the NF-κB-mediated cell death pathway. Using qRT-PCR analysis, we found that *Tnf*, *Nfkb2*, and *Nfkb1a* mRNA levels were markedly up-regulated in colonic epithelial cells in the *Mettl14* KO group, while the expression of the other genes related to TNF signaling did not change (Fig. 5E). Together, these data reveal that *Mettl14* suppresses TNF-induced cell death via the NF-κB-mediated antiapoptotic pathway.

### ***Nfkb1a* is the direct target of m<sup>6</sup>A modification in colonic epithelial cells**

To identify the direct target gene of m<sup>6</sup>A modification in colonic epithelial cells, we cross-referenced up-regulated genes from the bulk RNA-seq to four reported MeRIP-seq datasets obtained from the human gastrointestinal tract and cell lines (37). This analysis identified 366 overlapping genes in all datasets (Fig. 6A); among them, *Nfkb1a* was the only target of m<sup>6</sup>A modification that was involved in NF-κB pathway. We confirmed the MeRIP-seq data using m<sup>6</sup>A RNA immunoprecipitation qRT-PCR and found enrichment of m<sup>6</sup>A binding to *Nfkb1a* mRNA 3'UTR (Fig. 6B). It is well known that m<sup>6</sup>A modification enhances target mRNA degradation by addition of m<sup>6</sup>A modification to the 3'UTR region of the gene (39). Depletion of m<sup>6</sup>A modification resulted in the accumulation of *Nfkb1a* mRNA due to a lower rate of degradation than WT littermates, as confirmed by the RNA decay assay in which actinomycin D was used to block the mRNA transcription (Fig. 6C) (27). Furthermore, we found that *Nfkb1a* has a broad distribution and relatively higher expression in stem cells and TA cells by analyzing our scRNA-seq data (Fig. 6D). Meanwhile, the *Nfkb1a* mRNA level was up-regulated mostly in *Mettl14* KO stem cells and TA cells (Fig. 6E). In addition, the up-regulation of *Nfkb1a* mRNA expression resulted in a higher level of NFKB1A protein (Fig. 6F). It is known that increased levels of NFKB1A protein inhibit the canonical activity of NF-κB and promote TNF-stimulated cell death (17). Consistently, the expression of the proapoptotic protein Bax was increased, and expression of the antiapoptotic protein Bcl2 was decreased in *Mettl14* KO mice (Fig. 6F).

Given that TNF-induced cell death is dependent on the activity of receptor-interacting serine/threonine kinase 1 (RIPK1) (40), we investigated whether inhibition of RIPK1 activity can rescue the phenotype. Crypts isolated from *Mettl14* KO and *Mettl14* WT mice were incubated in a 3D organoid culture medium with or without the RIPK1 inhibitor GSK'963. We found that organoid-forming efficiency in the *Mettl14* KO group with GSK'963 was increased compared to the *Mettl14* KO group, while GSK'963 had no impact on the organoid formation in the *Mettl14* WT group (Fig. 6G), confirming that the *Mettl14* deficiency that led to colonic epithelial cell death was dependent on RIPK1 activity. Although Wnt signaling is indispensable for the differentiation and proliferation of intestinal stem cells, no differences in Wnt signaling were observed between *Mettl14* WT and *Mettl14* KO mice (fig. S6). Together, we conclude that m<sup>6</sup>A modification sustains colonic epithelial cell survival by regulating the stability of *Nfkb1a* mRNA and, therefore, modulates TNF-induced cell death via NF-κB activity.

## **DISCUSSION**

Our present study demonstrated that METTL14 is essential for maintaining colonic epithelial homeostasis by controlling epithelial cell death at steady state. *Mettl14* KO-mediated loss of m<sup>6</sup>A modification led to the accumulation of *Nfkb1a* mRNA and protein in intestinal epithelial cells, promoting cell death through the inhibition of NF-κB signaling, thus triggering the loss of colonic stem cells and resultant colitis. This is a comprehensive study focusing on the physiological function of METTL14 and m<sup>6</sup>A modification in colonic epithelial cells and stem cells.

Although a recent study reported that the modulation of translation by the m<sup>6</sup>A reader protein YTHDF1 affects intestinal tumorigenesis by targeting Wnt signaling (32), our work has delineated the novel function of the m<sup>6</sup>A “writer” METTL14 in intestinal epithelial cells under physiological conditions. Genetic ablation of the m<sup>6</sup>A writer protein METTL14 in mice resulted in a wasting phenotype and impairment of epithelial development at 2 weeks of age and spontaneous colitis in adults. *Ythdf1* KO mice did not exhibit an intestinal phenotype under normal conditions, while *Mettl14* KO mice spontaneously developed severe colon damage and had a lower survival rate than *Mettl14* WT mice. One possible explanation is that the METTL14-associated m<sup>6</sup>A writer complex adds m<sup>6</sup>A modification to a number of different target mRNAs and thus affects RNA metabolism, including decay, splicing, translocation, and translation, while *Ythdf1* recognizes only a few of the m<sup>6</sup>A-marked RNAs and mostly regulates the efficiency of the target RNA translation (41). To investigate whether *Mettl14* deficiency regulates intestinal epithelial cell differentiation, proliferation, and apoptosis, subsequently inducing the wasting phenotype and spontaneous colitis, we performed histological staining, qRT-PCR, scRNA-seq, and organoid culture analyses. However, we did not observe significant changes in the length of the small intestine, the integrity of the crypts, and the length of the villus, nor in the relative expression of specific markers of the different cell subsets in the small intestine, suggesting that the small intestine is not responsible for the marked wasting phenotype of the *Mettl14* KO. The *Mettl14* KO mice had a much higher colonic apoptotic rate and apoptosis-to-proliferation ratio than the WT mice, while no difference was seen in cell proliferation. In addition, *Mettl14*-deficient colonic crypts hardly survived in organoid culture, and a significant loss of stem cells was

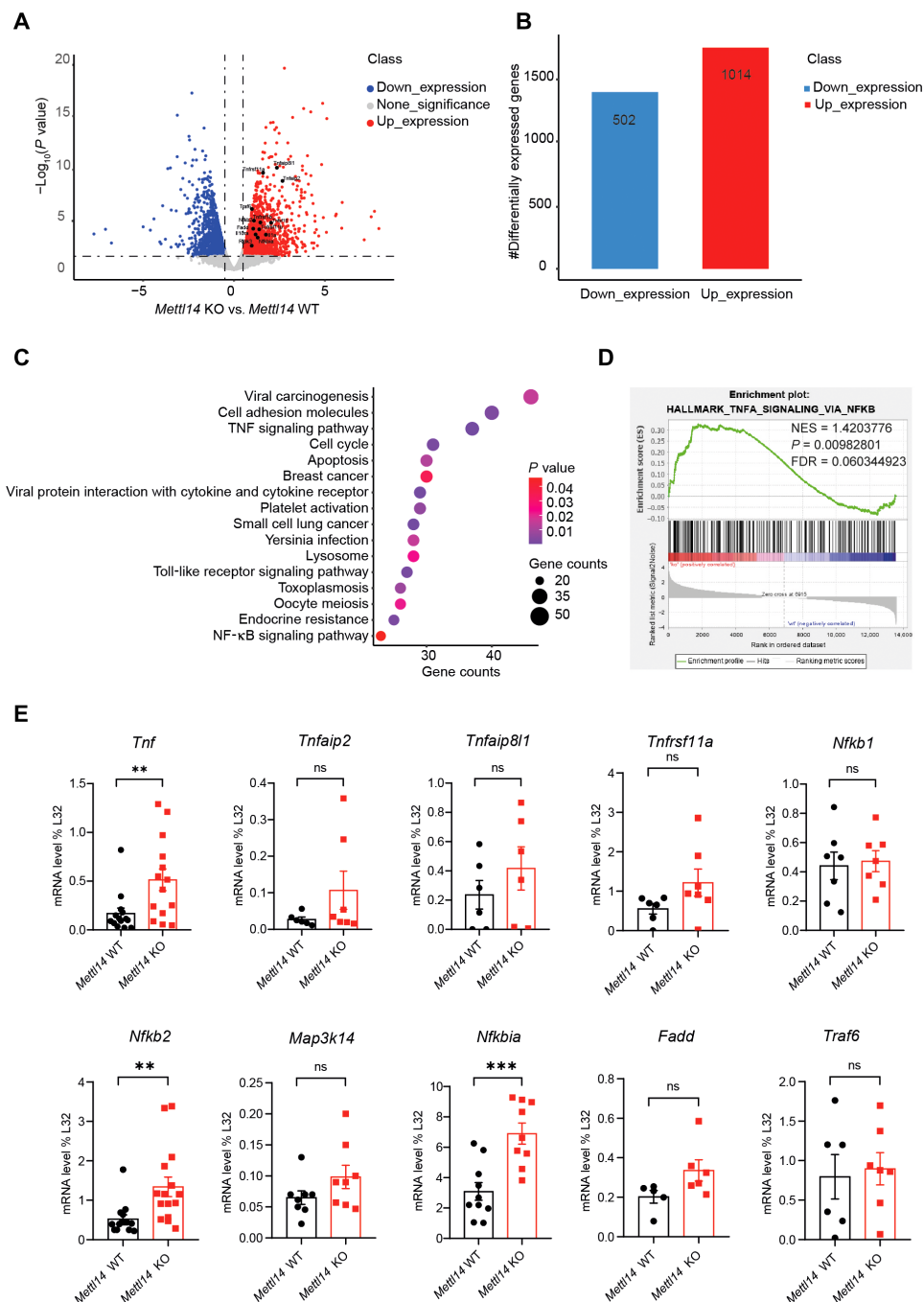


**Fig. 5.  $m^6A$  modification regulates colonic epithelial cell homeostasis by restricting TNF-induced cell death.** (A) Volcano plot of comparative RNA-seq data between 2-week-old *Mettl14* WT and *Mettl14* KO mice. The x axis specifies the  $\log_2$  fold changes (FC), and the y axis specifies the  $-\log_{10}$  P value (*Mettl14* KO compared to *Mettl14* WT). Blue dots represent down-regulated genes [ $\log_2(\text{FC}) \leq -1$  and  $P \leq 0.05$ ], and red dots represent up-regulated genes [ $\log_2(\text{FC}) \geq 1$  and  $P \leq 0.05$ ]. (B) Number of genes that increased significantly (red) and decreased (blue) in *Mettl14* KO versus *Mettl14* WT colonic epithelial cells. (C) KEGG enrichment analysis of differentially expressed genes. (D) GSEA plot determined by RNA-seq profiling. Analysis completed on genes ranked by  $\log_{10}$  false discovery rate (FDR) and FC sign, with enrichment determined after 1000 permutations. The statistics were computed using GSEA and controlled for multiple comparisons by FDR. NES, normalized enrichment score. (E) qRT-PCR was used to verify the differentially expressed genes related to the TNF signaling pathway ( $n = 6$  to 9 per group). Data are presented as means  $\pm$  SD. Two-sided Student's t test (E) was performed (\*\* $P < 0.01$ , \*\*\* $P < 0.001$ ).

found in the *Mettl14* KO mice compared with the WT group. Our scRNA-seq data show that *Mettl14* is highly expressed in stem cells and TA cells compared with other subsets in mice. Human Atlas studies indicate that METTL14 is expressed at much higher levels in differentiated cell enterocytes and secretory cells compared to stem

cells and TA cells. While this seems inconsistent to Human Atlas studies, our data are based on objective scRNA-seq of individual mice. This could be due to species differences between humans and mice, or due to the sampling timing, as we used 2-week-old pups for scRNA-seq, while the Human Atlas studies are mostly based on

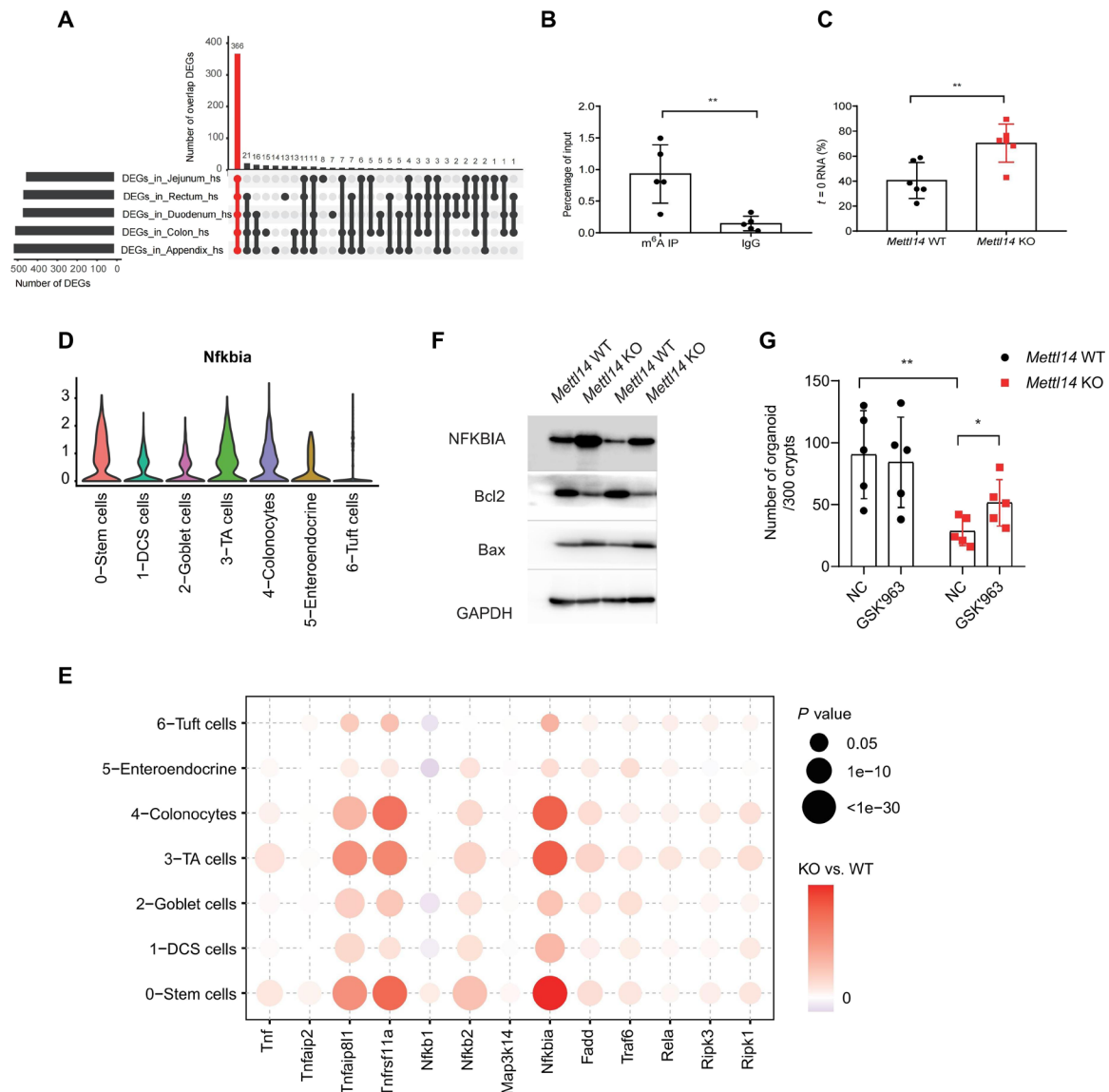


**Fig. 6. *Nfkbia* is the direct target of m<sup>6</sup>A modification in colonic epithelial cells.** (A) UpSet plot showed genes overlapped between the RNA-seq data and m<sup>6</sup>A RIP sequencing datasets. DEGs, differentially expressed genes. (B) mRNA isolated from colonic epithelial cells was immunoprecipitated (IP) with an anti-m<sup>6</sup>A antibody, and qRT-PCR was used to assess the mRNA level of *Nfkbia* ( $n = 5$  per group). (C) Colonic epithelial cells were treated with actinomycin D for 4 hours, and *Nfkbia* mRNA was normalized for 0 hours ( $n = 6$  per group). (D) Violin plot showing the distribution of *Nfkbia* per single cell in each cluster. (E) Bubble heatmap showing expression of TNF signaling pathway-related genes for each cluster. (F) Representative immunoblot for NFKBIA, Bcl2, and Bax in colonic epithelial cells from 2-week-old mice; glyceraldehyde-3-phosphate dehydrogenase (GAPDH) was used as a loading control. (G) Crypts isolated from *Mettl14* WT and *Mettl14* KO mice were grown in 3D organoid culture medium with or without RIPK1 inhibitor (GSK963, 1  $\mu$ M) ( $n = 5$  per group). Data are presented as means  $\pm$  SD. Two-sided Student's  $t$  test (B, C, and G) was performed (\*\* $P < 0.01$ ).

adult samples. Furthermore, *Mettl14* depletion in Lgr5<sup>+</sup> stem cells was more likely to promote a steady rate of apoptosis and DSS-induced colitis. Together, these data provide strong evidence that the colonic phenotype in *Mettl14* KO mice is mainly due to defects in the colonic stem cells and increased intestinal epithelial cell apoptosis.

We then explored the mechanism underlying the effects of the *Mettl14*-mediated m<sup>6</sup>A modification in colonic epithelial cell homeostasis and apoptosis. We found that *Mettl14* deficiency in intestinal epithelial cells promotes TNF-induced cell death by suppressing NF- $\kappa$ B-mediated antiapoptotic pathway. It has been shown that TNF binds to TNF receptor 1 (TNFR1) and forms the

TNFR1-associated signaling complex by recruiting cytoplasmic adaptor molecules, such as TNF receptor-associated death domain (TRADD), TNF receptor-associated factor 2 (TRAF2), RIPK1, and cellular inhibitors of apoptosis 1 and 2 (c-IAP1/2). The TNFR1-associated signaling complex rapidly activates IKK and degrades NFKBIA, and thus induces the activation of NF- $\kappa$ B signaling, which promotes survival and the inflammatory response. Inhibition of NF- $\kappa$ B by overexpression of nondegradable NFKBIA favors RIPK1-dependent cell death (17, 40). Similarly, our data show a much higher level of NFKBIA in *Mettl14* KO mice and that *Mettl14* deficiency led to colonic epithelial cell death in a manner dependent on RIPK1 activity.

Several studies on METTL14 suggest that its role in CRC is as an antitumor protein (42, 43), implying that METTL14 could inhibit intestinal epithelial cell proliferation, while our data mainly attributed METTL14 function to maintain intestinal epithelial cell survival. There could be several possible reasons: (i) The other studies mainly draw their conclusion based on in vitro studies with CRC cell lines, which were well known to contain a lot of gene mutations, such as *APC*, *KRAS*, *BRAF*, and *TP53*, that might interfere or synergize with METTL14 and led to different conclusions, and (ii) m<sup>6</sup>A is involved in almost every process of cell development, proliferation, apoptosis, and carcinogenesis. METTL14 may play completely different roles by different mechanisms in maintaining the homeostasis of colonic epithelial cells and in the occurrence and development of CRC. It is well known that Wnt signaling modulates the self-renewal and differentiation of intestinal stem cells (44). Han *et al.* (32) found that *Ythdf1* amplified Wnt signaling by targeting mRNA translation of *Tcf7l2* in colon tumors. However, Wnt signaling was not perturbed in *Mettl14* KO colonic epithelial cells (fig. S6), further indicating that *Mettl14* does not affect the differentiation and proliferation of stem cells. Another report showed that METTL3 facilitated the development of CRC by activating the m<sup>6</sup>A-GLUT1-mTORC1 axis (34), and transgenic *Mettl3*<sup>+/-</sup> mice had fewer tumors after azoxymethane/DSS treatment compared to their WT littermates. Our work focused on the specific function of METTL14 in colonic epithelial cells under normal conditions by analyzing the phenotype of *Mettl14* KO mice. Moreover, m<sup>6</sup>A modification regulates chromosome-associated regulatory RNAs, modulating both the chromatin status and transcription (45); this interaction adds further complexity to the regulatory network downstream of m<sup>6</sup>A. Thus, further study will be informative in understanding the molecular mechanism by which different modulators of m<sup>6</sup>A mRNA modification regulate the function and development of intestinal epithelial cells.

Collectively, our work demonstrates the critical role of *Mettl14* in maintaining the homeostasis of colonic epithelial cells. Deficiency of METTL14 and m<sup>6</sup>A modification in mice lead to severe colitis, though inhibiting the NF-κB-mediated antiapoptotic pathway, suggesting a potential therapeutic strategy for colitis intervention by modulating METTL14 and the NF-κB signaling machinery.

## MATERIALS AND METHODS

### Mice

*Mettl14*<sup>fl/fl</sup> mice were generated as previously described with CRISPR-Cas9 technology by insertion of two loxp sites into *Mettl14* genome loci (27). *Mettl14*<sup>fl/fl</sup> mice without *Villin-Cre* were used as WT controls (*Mettl14* WT) for *Mettl14* KO mice. *Mettl14*<sup>fl/fl</sup> mice were crossed with *Lgr5-eGFP-IRES-creERT2* (*Lgr5-Cre*) mice to generate *Mettl14* depletion in *Lgr5*<sup>+</sup> stem cells.

*Villin-Cre* (B6.Cg strain; stock no. 004586) and *Lgr5-eGFP-IRES-CreERT2* (B6.129P2 strain; stock no. 002120) mice were obtained from The Jackson Laboratory and had been backcrossed to C57BL/6N mice (Charles River Laboratories) for more than 10 generations. All of the KO and WT mice were sex- and age-matched littermates and were cohoused for any experiments described. All the mice were maintained under specific pathogen-free conditions and used in accordance with the animal experimental guidelines set by the Institutional Animal Care and Use Committee (IACUC). This study has been approved by the IACUC of the Shanghai Jiao Tong University School of Medicine (protocol no. A-2015-016) and the Shanghai Jiao Tong University (protocol no. 2017043).

### Isolation of mouse intestinal epithelial cells

For the isolation of colonic epithelial cells, the colon tissue was cut into 2-mm segments and incubated in RPMI 1640 medium containing 2.5 mM EDTA and 2% fetal serum albumin for 30 min at 4°C on a rocker. Epithelial cells were released by vigorous shaking and passed through a 70-μm strainer and then washed with cold Dulbecco's phosphate-buffered saline (DPBS) containing 2% fetal serum albumin.

### Mouse colonic organoid culture

IntestiCult Organoid Growth Medium (Mouse) (STEMCELL Technologies, catalog no. 06005) was used for the establishment and maintenance of mouse colonic organoids. Briefly, the mice were sacrificed and the colon was harvested from each mouse. The colon was flushed gently with cold PBS containing 1% fetal serum albumin. Small scissors were used to make a longitudinal incision along the entire length of the colon, and then the colon was cut into 2-mm pieces. A 10-ml serological pipette was used to wash the colonic pieces by pipetting up and down three times. The supernatant was removed. This wash procedure was repeated 15 to 20 times or until supernatant was clear. Then, the colonic pieces were suspended in 25-ml Gentle Cell Dissociation Reagent (STEMCELL Technologies, catalog no. 07174) in a shaker at 20 rpm for 20 min at room temperature. The colonic pieces were resuspended in 10 ml of cold PBS containing 0.1% bovine serum albumin and pipetted up and down three times, and the supernatant was passed through a 100-μm strainer into a 50-ml conical tube. This procedure was repeated six times, and the crypts were collected. The quality of the suspensions was assessed, and the crypt number was counted with an inverted microscope. Crypts were used for organoid development in domes made by Matrigel (Corning, catalog no. 356231) and IntestiCult Organoid Growth Medium (1:1). Suspension (50 μl) for each dome was pipetted into a 24-well plate. Next, the plate was incubated at 37°C for 10 to 15 min until the Matrigel was solidified. Last, 750 μl of complete IntestiCult Organoid Growth Medium was added to each well and incubated at 37°C and 5% CO<sub>2</sub>.

### RNA isolation and qRT-PCR

RNA was extracted using the TRIzol reagent (Invitrogen) and further purified using the RNase-Free DNase Set (QIAGEN, catalog no. 79256). The Maxima H Minus Reverse Transcriptase Kit (Thermo Fisher Scientific, catalog no. EP0753) was used for complementary DNA (cDNA) synthesis. The iTaq Universal SYBR Green Supermix was used for real-time PCR, and *L32* or *Hprt* mRNA level was used as internal control to calculate mRNA relative abundance. The primer sequences used for qPCR were as follows:

*Mettl14*: 5'-CTCCAAACTCAAAACGGAAGTGT-3' (forward) and 5'-ATGGGGATTTAAGCTCTGCGT-3' (reverse); *Vill1*: 5'-GCTTGCCACAACCTTCTAAGAT-3' (forward) and 5'-TCAGTTTAGTCATGGTGGACGA-3' (reverse); *Lgr5*: 5'-CCTACTCGAAGACTTACCCAGT-3' (forward) and 5'-GCATTGGGGTGAATGATAGCA-3' (reverse); *Gob5*: 5'-GGAAGGCAAAGCCTGAATAT-3' (forward) and 5'-GGCTCATCATTGCCTAGAGG-3' (reverse); *Alpi*: 5'-AGGACATCGCCACTCAACTC-3' (forward) and 5'-GGTTCAGACTGGTTACTGTCA-3' (reverse); *Chga*: 5'-CGATCCAGAAAGATGATGGTC-3' (forward) and 5'-CGGAAGCCTCTGTCTTCC-3' (reverse); *Tnf*: 5'-CCCTCACACTCAGATCATCTTCT-3' (forward) and 5'-GCTACGACGTGGGCTACAG-3' (reverse); *Tnfrsf25*: 5'-AGGAGGAGTCTGCGAAGAAGA-3' (forward) and 5'-GGCAGTGGACCATCTAACTCG-3' (reverse);

*Tnfrsf11a*: 5'-GTTTGTGGACAATACCAGCAGT-3' (forward) and 5'-GTTCTTCACTACCCTCTGTGC-3' (reverse); *Tnfrsf11a*: 5'-GGACGGTGTTCAGCAGAT-3' (forward) and 5'-GCAGTCTGAGTTCCAGTGGTA-3' (reverse); *Nfkb1*: 5'-GGAGGCATGTTCCGGTAGTGG-3' (forward) and 5'-CCCTGCGTTGGATTTTCGTG-3' (reverse); *Nfkb2*: 5'-AGTGTGCGCTGTGTCTGTAG-3' (forward) and 5'-GTTCTTCTTGGTTACATGCAGGA-3' (reverse); *Map3k14*: 5'-TGTGGGAAGTGGGAGATCCTA-3' (forward) and 5'-GGCTGAACTCTTGGCTATTCTCA-3' (reverse); *Nfkbia*: 5'-TGAAGGACGAGGAGTACGAGC-3' (forward) and 5'-TTCGTGGATGATTGCCAAGTG-3' (reverse); *Fadd*: 5'-GCGCCGACACGATCTACTG-3' (forward) and 5'-TTACCCGCTCACTCAGACTTC-3' (reverse); *Traf6*: 5'-AAAGCGAGAGATTCTTTCCCTG-3' (forward) and 5'-ACTGGGGA CAATTC ACTAGAGC-3' (reverse); *Nfkbia* for RIP: 5'-GCCAGCGTCTGACCATTATAAG-3' (forward) and 5'-ACTCTATTTGTACAAATATACAAGTCCAC-3' (reverse); *Ascl2*: 5'-AAGCACACCTTGACTGGTACG-3' (forward) and 5'-AAGTGGACGTTTGACCTTCA-3' (reverse); *Tcf7l2*: 5'-TCATCACGTACAGCAATGAACA-3' (forward) and 5'-CGACAGCGGGTAATATGGAGAG-3' (reverse); *Ephb2*: 5'-GCGGCTACGACGAGAACAT-3' (forward) and 5'-GGCTAAGTCAAAATCAGCCTCA-3' (reverse); *Axin2*: 5'-ATGAGTAGCGCCGTGTAGTG-3' (forward) and 5'-GGCATAGGTTTGGTGGACT-3' (reverse); *Hprt*: 5'-TCAGTCAACGGGGGACATAAA-3' (forward) and 5'-GGGGCTGTACTGCTTAACCAG-3' (reverse); *L32*: 5'-AAAAACAGACGCACCATCGAA-3' (forward) and 5'-TTCAGGTGACCACATTCAGGG-3' (reverse).

### Diarrhea analysis

We calculated the proportion of water in feces to determine the diarrhea situation of 2-week-old mice. Briefly, sterile 1.5-ml tubes were weighed, and stools were collected by these tubes and weighed. Then, the lid of the tubes was opened and the tubes were put on a constant temperature flat bed at 80°C overnight. The tubes were weighed again, and the reduced weight is water.

### Immunohistochemical and histological analysis

Mouse intestinal tissue segments were harvested and fixed in 10% formalin solution overnight at room temperature. Postfixation samples were moved to 70% ethanol and then sent to the Histology Core of the Shanghai Institute of Immunology for processing. Histological grading was performed by two blinded investigators as described previously (46). Briefly, the amount and depth of inflammation, crypt damage, or regeneration were used to grade the histological score. For immunohistochemical staining, the sections were deparaffinized and washed in PBS. Antigen retrieval was performed by heating the sections in 10 mM sodium citrate buffer (pH 6.0). The sections were washed in PBS after cooling, incubated in 3% hydrogen peroxide for 10 min at room temperature, and then washed again in PBS. The sections were blocked in PBS containing 1% bovine serum albumin for 1 hour at room temperature and stained in blocking buffer containing primary antibodies overnight at 4°C. On the following day, the sections were warmed to room temperature for 1 hour and stained with a horseradish peroxidase (HRP)-polymer complex for 20 min, followed by incubation with secondary antibody for 20 min. The sections were washed three times in PBS, developed with 3,3'-diaminobenzidine (DAB) reagent (Peroxidase Substrate Kit, ZSGB-BIO, catalog no. ZLI-9018), and counterstained with hematoxylin. The sections were washed with tap water and then subsequently washed with increasing ethanol concentrations for

dehydration. Once mounted and air-dried, the slices were viewed under Digital Whole Slide Scanner (Hamamatsu, NanoZoomer S360) and analyzed with NDP.view2 software. Tissue sections were assessed for pathology as previously described. The list of antibodies used in the immunohistochemical and histological analyses is shown in table S1.

### TUNEL staining

For TUNEL staining, colon sections were treated with a TUNEL kit (Sigma-Aldrich, St. Louis, MO, USA) according to the manufacturer's instructions. TUNEL-positive cells were observed under a confocal microscope (FLUOVIEW FV3000, Olympus) and analyzed with Imaris software.

### Immunofluorescence

Formalin-fixed paraffin-embedded tissue sections were deparaffinized, and antigen retrieval was performed by heating the sections in 10 mM sodium citrate buffer (pH 6.0). The sections were washed with PBS three times and then rinsed with PBS containing 0.5% Triton X-100 and 0.05% Tween 20 for 10 min. The sections were added in blocking buffer (PBS and 0.025% Triton X-100, 0.05% Tween 20, and 5% bovine serum albumin) for 30 min at room temperature. Primary antibodies were incubated overnight at 4°C, and the secondary antibodies were incubated for 1 hour at room temperature on the following day. The sections were mounted with Fluoroshield histology medium containing 4',6-diamidino-2-phenylindole (DAPI) (Sigma-Aldrich, F6057). The slices were viewed under a confocal microscope (FLUOVIEW FV3000, Olympus) and analyzed with Imaris software. The list of antibodies used in the immunofluorescence analysis is shown in table S1.

### DSS-induced colitis analysis

*Mettl14<sup>fl/fl</sup> Lgr5<sup>creERT</sup>* and *Mettl14<sup>fl/fl</sup>* WT control mice were treated with tamoxifen for 7 days and then rested for 7 days, and 2% DSS water was added. The weight of mice was observed at the same time point every day. On days 6 and 7, the severity of DSS-induced colitis was detected by endoscopy analysis. Stool, blood vessels, particle size, and translucency were used to evaluate the colitis score, and detailed scoring criteria were performed as described previously (47). The mice were euthanized on day 9, and the colon lengths were detected.

### Tamoxifen treatment

For *Mettl14<sup>fl/fl</sup> Lgr5<sup>creERT</sup>* mice, tamoxifen-inducible, Cre-mediated recombination will result in deletion of the floxed sequences in the *Lgr5*-expressing cells of the offspring. Tamoxifen was added to corn oil (20 mg/ml) and shaken overnight at 37°C protected from light. Mice were administered tamoxifen (75 mg/kg body weight) via intraperitoneal injection daily for 7 days and then rested for 3 days for cell apoptosis analysis or 7 days before DSS-induced colitis.

### Western blot

Total protein of colonic epithelial cells was extracted with radioimmunoprecipitation assay lysis buffer supplemented with protease inhibitors (Thermo Fisher Scientific). Antibodies against METTL14 (Sigma-Aldrich, catalog no. HPA038002), NFKBIA (Cell Signaling Technology, catalog no. 9242s), Bax (Cell Signaling Technology, catalog no. 2772), Bcl2 (ProteinTech, catalog no. 12789), and glyceraldehyde-3-phosphate dehydrogenase (GAPDH) (Cell Signaling Technology, catalog no. 2118) were used at a 1:1000 dilution in

5% nonfat milk buffer at 4°C overnight. After that, an HRP-conjugated secondary antibody (Cell Signaling Technology, catalog no. 7074) was incubated at room temperature for 1 hour. Signals were detected with an Immobilon Western HRP substrate (Millipore, WBKLS0500) and visualized using Amersham Imager 600 System (GE Healthcare Bio-Sciences) and quantified by gel analysis using ImageJ software (National Institutes of Health, USA).

### m<sup>6</sup>A-RIP-qPCR

m<sup>6</sup>A-RIP-qPCR analysis was conducted as described previously (48). Briefly, total RNA was isolated from colonic epithelial cells. Polyadenylated RNA was further enriched from total RNA by using the Dynabeads mRNA Purification Kit (Invitrogen) and incubated with anti-m<sup>6</sup>A antibody (Synaptic System, catalog no. 202003) or rabbit immunoglobulin G (IgG). The mixture was then immunoprecipitated by incubation with 50 µl of protein A beads (Sigma-Aldrich, P9424). After being washed three times, bound RNA was eluted from the beads with m<sup>6</sup>A (0.5 mg/ml; Berry & Associates, PR3732) and then extracted by TRIzol. qRT-PCR was conducted, and the expression of *Nfkbia* was normalized to the input sample. *Rps21* was chosen as the m<sup>6</sup>A-negative control, and *ptpn4* was chosen as the m<sup>6</sup>A-positive control (48).

### RNA decay analysis

Colonic epithelial cells from 2-week-old mice were plated on 96-well plates with  $1 \times 10^5$  cells per well. After treatment with actinomycin D (5 µg/ml) (Sigma-Aldrich, catalog no. A1410) for 4 hours, cells were collected and subjected to RNA extraction. Total RNA was isolated, and qRT-PCR was conducted for mRNA levels as described above.

### m<sup>6</sup>A dot-blot assay

mRNA was purified by a Dynabeads mRNA purification kit (Ambion, 61006) and quantified using ultraviolet spectrophotometry. The m<sup>6</sup>A dot blot was performed on Bio-Dot Apparatus (Bio-Rad, no. 170-6545). In brief, the primary rabbit anti-m<sup>6</sup>A antibody (Synaptic Systems, 202003) was applied to the charged nylon-based membrane containing mRNA samples. HRP-conjugated goat anti-rabbit IgG (DakoCytomation, p0448) was added to the blots and then developed with enhanced chemiluminescence (GE Healthcare, RPN2232). The signal density of the dot-blot experiment is quantified with Gel-Pro analyzer software (Media Cybernetics) in all experiments.

### RNA sequencing

The colonic epithelial cells were isolated from 2-week-old mice as described above. RNA was extracted using the TRIzol reagent (Invitrogen) according to the manufacturer's instructions. Libraries were constructed and sequenced using the BGISEQ-500 sequencer. Raw sequencing reads were cleaned by removing adaptor sequences, reads containing poly-N sequences, and low-quality reads, and clean reads were then mapped to GenBank to identify known mouse mRNA. RNA-seq and analysis were conducted by OE Biotech Co. Ltd.

### scRNA-seq and data analysis

Colonic epithelial cells were stained with an EpCAM and live/dead cell kit (Thermo Fisher Scientific, catalog no. L34965) on ice in the dark for 30 min. The EpCAM<sup>+</sup> live cells were sorted by flow cytometry (Beckman Coulter MoFlo Astrios EQ), and cell number was counted. The cells were diluted to a final concentration range of 250 to

400 cells/µl for single-cell sequencing according to the manufacturer's instructions (10x Genomics kit, chromium single cell 3' reagent kits V2) (49). For analysis of single-cell data, a total of 7863 cells after filtering and removing immune clusters were used. The raw sequencing reads from 10x Genomics 3-prime sequencing were processed with Cell Ranger (50) to generate gene-cell count matrices. This matrix was filtered, retaining cells with more than 500 genes and less than 20% mitochondria transcripts; genes expressed more than five cells. Datasets from *Mettl14* WT and *Mettl14* KO samples were integrated with Seurat using canonical correlation analysis (CCA) with Seurat (51). The top 15 CCA components were aligned to remove batch effect. Seurat was also used for data normalization with log (counts per 10,000 + 1), scaling, dimension reduction, clustering, and marker gene identification (Wilcoxon test by default). *t*-SNE was used for 2D visualization. We removed clusters of immune cells based on the expression of gene *Ptpcr* (CD45) and retained only nonimmune cells. Clusters of the same cell types were merged together. To better inspect the gene expression distribution of modulators of m<sup>6</sup>A modification, which have relatively low expression and tend to have more dropout (52), we used ALRA (53) to impute the merged expression matrix from WT and KO samples in Fig. 4D.

### Statistical analysis

Statistical analysis was performed with GraphPad Prism 8.01. Unpaired Student's *t* test and two-tailed Mann-Whitney *U* test were used for measurement data of two-group analysis. One-way analysis of variance (ANOVA) was used for measurement data of more than two groups. All general statistical analysis was calculated with a confidence interval of 95%. *P* values  $\leq 0.05$  were considered as statistically significant (\**P* < 0.05; \*\**P* < 0.01; \*\*\**P* < 0.001; \*\*\*\**P* < 0.0001). Survival curves were compared by the log-rank test. Data are represented as means  $\pm$  SD as indicated in the figures. All authors had access to the data and reviewed and approved the final manuscript.

### SUPPLEMENTARY MATERIALS

Supplementary material for this article is available at <https://science.org/doi/10.1126/sciadv.abl5723>

[View/request a protocol for this paper from Bio-protocol.](#)

### REFERENCES AND NOTES

1. H. Clevers, The intestinal crypt, a prototype stem cell compartment. *Cell* **154**, 274–284 (2013).
2. L. G. van der Flier, H. Clevers, Stem cells, self-renewal, and differentiation in the intestinal epithelium. *Annu. Rev. Physiol.* **71**, 241–260 (2009).
3. A. Velcich, W. Yang, J. Heyer, A. Fragale, C. Nicholas, S. Viani, R. Kucherlapati, M. Lipkin, K. Yang, L. Augenlicht, Colorectal cancer in mice genetically deficient in the mucin *Muc2*. *Science* **295**, 1726–1729 (2002).
4. H. F. Farin, J. H. Van Es, H. Clevers, Redundant sources of Wnt regulate intestinal stem cells and promote formation of Paneth cells. *Gastroenterology* **143**, 1518–1529.e7 (2012).
5. N. Sasaki, N. Sachs, K. Wiebrands, S. I. Ellenbroek, A. Fumagalli, A. Lyubimova, H. Begthel, M. van den Born, J. H. van Es, W. R. Karthaus, V. S. Li, C. Lopez-Iglesias, P. J. Peters, J. van Rheenen, A. van Oudenaarden, H. Clevers, Reg4<sup>+</sup> deep crypt secretory cells function as epithelial niche for Lgr5<sup>+</sup> stem cells in colon. *Proc. Natl. Acad. Sci. U.S.A.* **113**, E5399–E5407 (2016).
6. C. L. May, K. H. Kaestner, Gut endocrine cell development. *Mol. Cell. Endocrinol.* **323**, 70–75 (2010).
7. M. Bjerknes, C. Khandanpour, T. Moroy, T. Fujiyama, M. Hoshino, T. J. Klisch, Q. Ding, L. Gan, J. Wang, M. G. Martin, H. Cheng, Origin of the brush cell lineage in the mouse intestinal epithelium. *Dev. Biol.* **362**, 194–218 (2012).
8. K. J. Maloy, F. Powrie, Intestinal homeostasis and its breakdown in inflammatory bowel disease. *Nature* **474**, 298–306 (2011).
9. N. D. Perkins, Achieving transcriptional specificity with NF-kappa B. *Int. J. Biochem. Cell Biol.* **29**, 1433–1448 (1997).

10. N. D. Perkins, The Rel/NF- $\kappa$ B family: Friend and foe. *Trends Biochem. Sci.* **25**, 434–440 (2000).
11. S. Ghosh, M. Karin, Missing pieces in the NF- $\kappa$ B puzzle. *Cell* **109**, S81–S96 (2002).
12. A. A. Beg, W. C. Sha, R. T. Bronson, S. Ghosh, D. Baltimore, Embryonic lethality and liver degeneration in mice lacking the RelA component of NF- $\kappa$ B. *Nature* **376**, 167–170 (1995).
13. J. A. Dominguez, A. J. Samocha, Z. Liang, E. M. Burd, A. B. Farris, C. M. Coopersmith, Inhibition of IKK $\beta$  in enterocytes exacerbates sepsis-induced intestinal injury and worsens mortality. *Crit. Care Med.* **41**, e275–e285 (2013).
14. L. J. Egan, L. Eckmann, F. R. Greten, S. Chae, Z. W. Li, G. M. Myhre, S. Robine, M. Karin, M. F. Kagnoff, IkappaB-kinasebeta-dependent NF- $\kappa$ B activation provides radioprotection to the intestinal epithelium. *Proc. Natl. Acad. Sci. U.S.A.* **101**, 2452–2457 (2004).
15. F. R. Greten, L. Eckmann, T. F. Greten, J. M. Park, Z. W. Li, L. J. Egan, M. F. Kagnoff, M. Karin, IKKbeta links inflammation and tumorigenesis in a mouse model of colitis-associated cancer. *Cell* **118**, 285–296 (2004).
16. L. W. Chen, L. Egan, Z. W. Li, F. R. Greten, M. F. Kagnoff, M. Karin, The two faces of IKK and NF- $\kappa$ B inhibition: Prevention of systemic inflammation but increased local injury following intestinal ischemia-reperfusion. *Nat. Med.* **9**, 575–581 (2003).
17. S. Y. Lee, D. R. Kaufman, A. L. Mora, A. Santana, M. Boothby, Y. Choi, Stimulus-dependent synergism of the antiapoptotic tumor necrosis factor receptor-associated factor 2 (TRAF2) and nuclear factor kappaB pathways. *J. Exp. Med.* **188**, 1381–1384 (1998).
18. R. Desrosiers, K. Friderici, F. Rottman, Identification of methylated nucleosides in messenger RNA from Novikoff hepatoma cells. *Proc. Natl. Acad. Sci. U.S.A.* **71**, 3971–3975 (1974).
19. D. Dominissini, S. Moshitch-Moshkovitz, S. Schwartz, M. Salmon-Divon, L. Ungar, S. Osenberg, K. Cesarkas, J. Jacob-Hirsch, N. Amariglio, M. Kupiec, R. Sorek, G. Rechavi, Topology of the human and mouse m6A RNA methylomes revealed by m6A-seq. *Nature* **485**, 201–206 (2012).
20. K. D. Meyer, Y. Saleatore, P. Zumbo, O. Elemento, C. E. Mason, S. R. Jaffrey, Comprehensive analysis of mRNA methylation reveals enrichment in 3' UTRs and near stop codons. *Cell* **149**, 1635–1646 (2012).
21. G. Jia, Y. Fu, X. Zhao, Q. Dai, G. Zheng, Y. Yang, C. Yi, T. Lindahl, T. Pan, Y. G. Yang, C. He, N6-methyladenosine in nuclear RNA is a major substrate of the obesity-associated FTO. *Nat. Chem. Biol.* **7**, 885–887 (2011).
22. G. Zheng, J. A. Dahl, Y. Niu, P. Fedorcsak, C. M. Huang, C. J. Li, C. B. Vagbo, Y. Shi, W. L. Wang, S. H. Song, Z. Lu, R. P. Bosmans, Q. Dai, Y. J. Hao, X. Yang, W. M. Zhao, W. M. Tong, X. J. Wang, F. Bogdan, K. Furu, Y. Fu, G. Jia, X. Zhao, J. Liu, H. E. Krokan, A. Klungland, Y. G. Yang, C. He, ALKBH5 is a mammalian RNA demethylase that impacts RNA metabolism and mouse fertility. *Mol. Cell* **49**, 18–29 (2013).
23. J. Liu, Y. Yue, D. Han, X. Wang, Y. Fu, L. Zhang, G. Jia, M. Yu, Z. Lu, X. Deng, Q. Dai, W. Chen, C. He, A METTL3-METTL14 complex mediates mammalian nuclear RNA N6-adenosine methylation. *Nat. Chem. Biol.* **10**, 93–95 (2014).
24. P. Wang, K. A. Doxtader, Y. Nam, Structural basis for cooperative function of Mettl3 and Mettl14 methyltransferases. *Mol. Cell* **63**, 306–317 (2016).
25. P. J. Batista, B. Molinie, J. Wang, K. Qu, J. Zhang, L. Li, D. M. Bouley, E. Lujan, B. Haddad, K. Daneshvar, A. C. Carter, R. A. Flynn, C. Zhou, K. S. Lim, P. Dedon, M. Wernig, A. C. Mullen, Y. Xing, C. C. Giallourakis, H. Y. Chang, m6A RNA modification controls cell fate transition in mammalian embryonic stem cells. *Cell Stem Cell* **15**, 707–719 (2014).
26. Q. J. Yao, L. Sang, M. Lin, X. Yin, W. Dong, Y. Gong, B. O. Zhou, Mettl3-Mettl14 methyltransferase complex regulates the quiescence of adult hematopoietic stem cells. *Cell Res.* **28**, 952–954 (2018).
27. H. B. Li, J. Tong, S. Zhu, P. J. Batista, E. E. Duffy, J. Zhao, W. Bailis, G. Cao, L. Kroehling, Y. Chen, G. Wang, J. P. Broughton, Y. G. Chen, Y. Kluger, M. D. Simon, H. Y. Chang, Z. Yin, R. A. Flavell, m6A mRNA methylation controls T cell homeostasis by targeting the IL-7/STAT5/SOCS pathways. *Nature* **548**, 338–342 (2017).
28. J. Tong, G. Cao, T. Zhang, E. Sefik, M. C. Amezcua Vesely, J. P. Broughton, S. Zhu, H. Li, B. Li, L. Chen, H. Y. Chang, B. Su, R. A. Flavell, H. B. Li, m6A mRNA methylation sustains Treg suppressive functions. *Cell Res.* **28**, 253–256 (2018).
29. K. J. Yoon, F. R. Ringeling, C. Vissers, F. Jacob, M. Pokrass, D. Jimenez-Cyrus, Y. Su, N. S. Kim, Y. Zhu, L. Zheng, S. Kim, X. Wang, L. C. Dore, P. Jin, S. Regot, X. Zhuang, S. Canzar, C. He, G. L. Ming, H. Song, Temporal control of mammalian cortical neurogenesis by m6A methylation. *Cell* **171**, 877–889.e17 (2017).
30. H. Weng, H. Huang, H. Wu, X. Qin, B. S. Zhao, L. Dong, H. Shi, J. Skibbe, C. Shen, C. Hu, Y. Sheng, Y. Wang, M. Wunderlich, B. Zhang, L. C. Dore, R. Su, X. Deng, K. Ferchen, C. Li, M. Sun, Z. Lu, X. Jiang, G. Marcucci, J. C. Mulloy, J. Yang, Z. Qian, M. Wei, C. He, J. Chen, METTL14 inhibits hematopoietic stem/progenitor differentiation and promotes leukemogenesis via mRNA m6A modification. *Cell Stem Cell* **22**, 191–205.e9 (2018).
31. M. Chen, L. Wei, C.-T. Law, F. H.-C. Tsang, J. Shen, C. L.-H. Cheng, L.-H. Tsang, D. W.-H. Ho, D. K.-C. Chiu, J. M.-F. Lee, C. C.-L. Wong, I. O.-L. Ng, C.-M. Wong, RNA N6-methyladenosine methyltransferase-like 3 promotes liver cancer progression through YTHDF2-dependent posttranscriptional silencing of SOCS2. *Hepatology* **67**, 2254–2270 (2018).
32. B. Han, S. Yan, S. Wei, J. Xiang, K. Liu, Z. Chen, R. Bai, J. Sheng, Z. Xu, X. Gao, YTHDF1-mediated translation amplifies Wnt-driven intestinal stemness. *EMBO Rep.* **21**, e49229 (2020).
33. H. Chen, S. Gao, W. Liu, C.-C. Wong, J. Wu, J. Wu, D. Liu, H. Gou, W. Kang, J. Zhai, C. Li, H. Su, S. Wang, F. Soares, J. Han, H. H. He, J. Yu, RNA N6-methyladenosine methyltransferase METTL3 facilitates colorectal cancer by activating m6A-GLUT1-mTORC1 axis and is a therapeutic target. *Gastroenterology* **160**, 1284–1300.e16 (2021).
34. Q. Wang, C. Chen, Q. Ding, Y. Zhao, Z. Wang, J. Chen, Z. Jiang, Y. Zhang, G. Xu, J. Zhang, J. Zhou, B. Sun, X. Zou, S. Wang, METTL3-mediated m6A modification of HDGF mRNA promotes gastric cancer progression and has prognostic significance. *Gut* **69**, 1193–1205 (2020).
35. M. E. Rothenberg, Y. Nusse, T. Kalisky, J. J. Lee, P. Dalerba, F. Scheeren, N. Lobo, S. Kulkarni, S. Sim, D. Qian, P. A. Beachy, P. J. Pasricha, S. R. Quake, M. F. Clarke, Identification of a cKit(+) colonic crypt base secretory cell that supports Lgr5(+) stem cells in mice. *Gastroenterology* **142**, 1195–1205.e6 (2012).
36. Y. Hayakawa, M. Tsuboi, S. Asfaha, H. Kinoshita, R. Niikura, M. Konishi, M. Hata, Y. Oya, W. Kim, M. Middelhoff, Y. Hikiba, N. Higashijima, S. Ihara, T. Ushiku, M. Fukayama, Y. Tailor, Y. Hirata, C. Guha, K. S. Yan, K. Koike, T. C. Wang, BHLHA15-positive secretory precursor cells can give rise to tumors in intestine and colon in mice. *Gastroenterology* **156**, 1066–1081.e16 (2019).
37. J. Liu, K. Li, J. Cai, M. Zhang, X. Zhang, X. Xiong, H. Meng, X. Xu, Z. Huang, J. Peng, J. Fan, C. Yi, Landscape and regulation of m6A and m6Am methylome across human and mouse tissues. *Mol. Cell* **77**, 426–440.e6 (2020).
38. Z. W. Li, W. Chu, Y. Hu, M. Delhase, T. Deerinck, M. Ellisman, R. Johnson, M. Karin, The IKKbeta subunit of IkappaB kinase (IKK) is essential for nuclear factor kappaB activation and prevention of apoptosis. *J. Exp. Med.* **189**, 1839–1845 (1999).
39. X. Wang, Z. Lu, A. Gomez, G. C. Hon, Y. Yue, D. Han, Y. Fu, M. Parisien, Q. Dai, G. Jia, B. Ren, T. Pan, C. He, N6-methyladenosine-dependent regulation of messenger RNA stability. *Nature* **505**, 117–120 (2014).
40. O. Micheau, J. Tschopp, Induction of TNF receptor I-mediated apoptosis via two sequential signaling complexes. *Cell* **114**, 181–190 (2003).
41. X. Wang, B. S. Zhao, I. A. Roundtree, Z. Lu, D. Han, H. Ma, X. Weng, K. Chen, H. Shi, C. He, N6-methyladenosine modulates messenger RNA translation efficiency. *Cell* **161**, 1388–1399 (2015).
42. X. Chen, M. Xu, X. X. K. Zeng, X. Liu, L. Sun, B. Pan, B. He, Y. Pan, H. Sun, X. Xia, S. Wang, METTL14 suppresses CRC progression via regulating N6-methyladenosine-dependent primary miR-375 processing. *Mol. Ther.* **28**, 599–612 (2020).
43. X. Yang, S. Zhang, C. He, P. Xue, L. Zhang, Z. He, L. Zang, B. Feng, J. Sun, M. Zheng, METTL14 suppresses proliferation and metastasis of colorectal cancer by down-regulating oncogenic long non-coding RNA XIST. *Mol. Cancer* **19**, 46 (2020).
44. C. Crosnier, D. Stamatakis, J. Lewis, Organizing cell renewal in the intestine: Stem cells, signals and combinatorial control. *Nat. Rev. Genet.* **7**, 349–359 (2006).
45. J. Liu, X. Dou, C. Chen, C. Chen, C. Liu, M. M. Xu, S. Zhao, B. Shen, Y. Gao, D. Han, C. He, N6-methyladenosine of chromosome-associated regulatory RNA regulates chromatin state and transcription. *Science* **367**, 580–586 (2020).
46. L. A. Dieleman, M. J. Palmen, H. Akol, E. Bloemena, A. S. Peña, S. G. Meuwissen, E. P. Van Rees, Chronic experimental colitis induced by dextran sulphate sodium (DSS) is characterized by Th1 and Th2 cytokines. *Clin. Exp. Immunol.* **114**, 385–391 (1998).
47. T. Kodani, A. Rodriguez-Palacios, D. Corridoni, L. Lopetuso, L. Di Martino, B. Marks, J. Pizarro, T. Pizarro, A. Chak, F. Cominelli, Flexible colonoscopy in mice to evaluate the severity of colitis and colorectal tumors using a validated endoscopic scoring system. *J. Vis. Exp.* **80**, e50843 (2013).
48. D. Dominissini, S. Moshitch-Moshkovitz, M. Salmon-Divon, N. Amariglio, G. Rechavi, Transcriptome-wide mapping of N6-methyladenosine by m6A-seq based on immunocapturing and massively parallel sequencing. *Nat. Protoc.* **8**, 176–189 (2013).
49. A. L. Haber, M. Biton, N. Rogel, R. H. Herbst, K. Shekhar, C. Smillie, G. Burgin, T. M. Delorey, M. R. Howitt, Y. Katz, I. Tirosh, S. Beyaz, D. Dionne, M. Zhang, R. Raychowdhury, W. S. Garrett, O. Rozenblatt-Rosen, H. N. Shi, O. Yilmaz, R. J. Xavier, A. Regev, A single-cell survey of the small intestinal epithelium. *Nature* **551**, 333–339 (2017).
50. G. X. Zheng, J. M. Terry, P. Belgrader, P. Ryvkin, Z. W. Bent, R. Wilson, S. B. Ziraldo, T. D. Wheeler, G. P. McDermott, J. Zhu, M. T. Gregory, J. Shuga, L. Montesclaros, J. G. Underwood, D. A. Masquelier, S. Y. Nishimura, M. Schnall-Levin, P. W. Wyatt, C. M. Hindson, R. Bharadwaj, A. Wong, K. D. Ness, L. W. Beppu, H. J. Deeg, C. McFarland, K. R. Loeb, W. J. Valente, N. G. Ericson, E. A. Stevens, J. P. Radich, T. S. Mikkelsen, B. J. Hindson, J. H. Bielas, Massively parallel digital transcriptional profiling of single cells. *Nat. Commun.* **8**, 14049–14060 (2017).
51. A. Butler, P. Hoffman, P. Smibert, E. Papalexi, R. Satija, Integrating single-cell transcriptomic data across different conditions, technologies, and species. *Nat. Biotechnol.* **36**, 411–420 (2018).

52. E. Pierson, C. Yau, ZIFA: Dimensionality reduction for zero-inflated single-cell gene expression analysis. *Genome Biol.* **16**, 241–250 (2015).
53. G. C. Linderman, J. Zhao, Y. Kluger, Zero-preserving imputation of scRNA-seq data using low-rank approximation. bioRxiv 397588 [Preprint], 22 August 2018. <https://doi.org/10.1101/397588>.

**Acknowledgments:** We would like to thank M. Yang, S. Hu, Y. Zhou, J. Alderman, C. Lieber, P. Ranney, L. Evangelisti, C. Hughes, and E. Hughes-Picard for technical and administrative assistance. We would like to thank all members of the Li laboratory and the Flavell laboratory for discussion. We would like to thank the flow core, sequencing core, and imaging core of Shanghai Institute of Immunology for their support. **Funding:** This work was supported by the National Natural Science Foundation of China (32070917/82030042/91753141 to H.-B.L. and 31800733 to T.Z.), the Shanghai Science and Technology Committee (20JC1417400/201409005500/20JC1410100 to H.-B.L.), the Program for Professor of Special Appointment (Eastern Scholar) at Shanghai Institutions of Higher Learning (H.-B.L.), the start-up fund from the Shanghai Jiao Tong University School of Medicine (H.-B.L.), and the Howard Hughes Medical Institute (R.A.F.).

**Author contributions:** T.Z. performed the experiments. C.D. performed part of experiments.

Z.C., B.C., and K.M. aided in some animal experiments. Y.H. aided in the experiments of m<sup>5</sup>A RIP qRT-PCR and m<sup>6</sup>A dot plot. T.Z. and C.D. analyzed the data and wrote the paper. T.Z., C.D., M.R., H.X., Y.K., Q.Z., Y.Y., M.Z., H.-B.L., and R.A.F. discussed the project and manuscript. H.-B.L. supervised the project and revised the paper. All authors approved the paper. **Competing interests:** R.A.F. is an advisor to GlaxoSmithKline, Zai Lab, and Ventus Therapeutics. All the other authors declare that they have no competing interests. **Data and materials availability:** All data needed to evaluate the conclusions in the paper are present in the paper and/or the Supplementary Materials. Sequencing reads are available in the National Center for Biotechnology Information (NCBI) Gene Expression Omnibus (GEO) database (accession no. GSE171423). The floxed Mett14 mouse strains can be provided by H.-B.L. pending scientific review and a completed material transfer agreement. Request for this mouse line should be submitted to H.-B.L. ([huabing.li@shsmu.edu.cn](mailto:huabing.li@shsmu.edu.cn)).

Submitted 22 July 2021

Accepted 2 February 2022

Published 25 March 2022

10.1126/sciadv.abl5723